Modeling of ionization of argon in an analytical capacitively coupled radio-frequency glow discharge

Annemie Bogaerts,[a] Min Yan, and Renaat Gijbels
Department of Chemistry, University of Antwerp (UIA), Universiteitsplein 1, B-2610 Wilrijk-Antwerp, Belgium

Wim Goedheer
FOM-Institute for Plasma Physics ''Rijnhuizen,'' P.O. Box 1207, 3430 BE Nieuwegein, The Netherlands

(Received 10 May 1999; accepted for publication 14 June 1999)

A hybrid Monte Carlo-fluid model has been developed for the description of electrons, argon ions, and fast argon atoms in a capacitively coupled radio-frequency (rf) glow discharge used in analytical spectroscopy. Typical operating conditions are about 6 Torr pressure and 10 W electrical power. The discharge cell is rather small and is characterized by a much smaller rf-powered electrode than grounded electrode, which yields a high dc bias voltage. The electron density at these conditions is in the order of $10^{13}\,\mathrm{cm}^{-3}$. The computation time to simulate all these electrons with a Monte Carlo or a particle-in-cell method was found to be too long. Therefore, the electrons are subdivided in two groups. The fast electrons emitted from the rf electrode, as well as the ones formed by ionization with sufficiently high total (=kinetic+potential) energy for further ionization, give rise to so-called γ ionization; these are described with a Monte Carlo method. The slow electrons, which can, however, be heated again by the fluctuating electric field, give rise to so-called α ionization; they are described with a fluid approach, which also treats the argon ions. Moreover, the fast argon ions and atoms are treated with a Monte Carlo model in the rf sheath. Typical results of this model include the electrical characteristics (i.e., dc bias and rf amplitude voltages, electrical current, potential, and electric field distributions), the electron densities and mean energies, the ionization rates due to the electron impact α and γ ionization and fast argon ion and atom impact ionization, and the relative contributions of these ionization mechanisms to the overall ionization. © *1999 American Institute of Physics.* [S0021-8979(99)07718-X]

I. INTRODUCTION

Glow discharges are used in a variety of application fields, including the microelectronics industry (for etching and deposition purposes), the laser and light industry, flat plasma display panel technology, etc. Moreover, they also find application in analytical chemistry, as a spectroscopic source for the analysis of solid materials by means of mass spectrometry or optical emission spectrometry. For the latter purpose, the material to be analyzed is used as the cathode of the glow discharge, which is sputtered by plasma species. The sputtered atoms arrive in the plasma, where they can be ionized or excited. The ions can then be detected by a mass spectrometer, and the excited atoms emit characteristic photons which can be measured with an optical emission spectrometer. It may seem that this method of using the sample to be analyzed as the cathode restricts the application of analytical glow discharges to conducting materials, because nonconducting materials would be charged up by the positive ion bombardment. However, nonconducting materials can also be analyzed by glow discharges, if the latter are operated in the radio-frequency (rf) mode. Indeed, the positive charge accumulated due to ion bombardment will then be neutralized by negative charge accumulation due to electron bombardment during part of the rf cycle. In recent years, rf glow discharges have gained increasing interest in analytical chemistry.[1–11] Typical working conditions are 13.56 MHz rf, several watts incoming power, a pressure of a few Torr, and voltages (both rf amplitude and dc bias) of about 500–1000 V. The analytical glow discharge cells are usually rather small, with typical dimensions of a few mm's electrode diameter and several cm's length.

In order to obtain a better insight into the glow discharge behavior, we have developed a set of two-dimensional models for a direct current (dc) glow discharge, consisting of various submodels (Monte Carlo, fluid, and collisional-radiative models) for describing various plasma species (electrons, argon ions, fast argon atoms, argon atoms in various excited levels, sputtered atoms and the corresponding ions, in the ground state and in various excited levels) (e.g.,[12–22]). Now we intend to construct a similar model setup for the analytical rf glow discharge. Recently, we have developed a hybrid Monte Carlo-fluid model for the electrons and argon ions[23] and a Monte Carlo model for the argon ions and fast argon atoms[24] in an analytical rf glow discharge. However, when the modeling results were compared to the modeling results for a dc glow discharge at similar conditions, we found that the ionization in the rf case was lower than in the dc case. This is in contrast to the general statements that an rf discharge yields more efficient ionization due to the back and forth movement of the electrons in the

[a]Electronic mail: bogaerts@uia.ua.ac.be

fluctuating electric field.[25,26] This discrepancy indicated that the ionization was not correctly described in our electron Monte Carlo model.

In the latter model, the electron behavior was simulated as a function of time in the rf cycle. Both the electrons starting at the rf electrode, and the electrons formed by ionization in the plasma, were followed. We checked how many rf cycles needed to be followed before periodic steady state was reached (the effect of all previous rf cycles was correctly taken into account in the results of the last rf cycle). This was found to be the case already for two rf cycles.[23] Indeed, the amount of ionization calculated with this Monte Carlo method was exactly the same when following 2 or 4 or 6 or 10 cycles. It seemed that at the discharge conditions under study (10 W power, 6 Torr pressure, rf-amplitude voltage of ~900 V and dc bias voltage around 600 V), the contribution of ionization due to slow electrons in the bulk plasma (so-called α ionization) was negligible compared to ionization due to electrons emitted by the rf electrode and accelerated in the strong electric field in the rf sheath (so-called γ ionization).

However, recently we realized that, when following only about 10 cycles, the electrons in the bulk plasma had not yet reached their full density, and when we followed the electrons during hundreds and thousands of rf cycles, their density still increased and their contribution in ionization really became important. Indeed, the energy they gain due to wave riding in the fluctuating electric field is not that large, but this electron group is so high in number, that they still play a significant role in the ionization. Hence, it appears that the analytical rf glow discharge operates in the transition region where both α and γ ionization play a role.

The relative importance of α and γ ionization, and the transition between the two regimes, have been studied, both by experimentalists and modelers, in Refs. 27–39. The existence of the two distinct regimes was first demonstrated by Levitskii and co-workers,[27] and has been experimentally and theoretically verified by Godyak and Kanneh[29] in terms of sharp changes in the density, current, sheath length, and electron temperature. Later on, the latter group also used a high-resolution Langmuir probe technique to measure the evolution of the electron energy distribution function from the α to the γ regime.[37] Another experiment by Vidaud and co-workers[32] involved the observation of visible light emission from γ and α discharges. The transition between the α and γ regimes has also been investigated by means of various models: analytical models,[29,39] self-consistent fluid models,[34,38] Monte Carlo simulations,[30] and a particle-in-cell Monte Carlo approach.[36] However, these models were generally applied to other conditions than our analytical glow discharge (e.g., lower gas pressure, lower frequency, lower voltage, other discharge gas, and generally larger cell geometry).

In order to correctly take into account the α ionization, we recently modified our electron Monte Carlo model, so that the electrons would be followed for many more rf cycles. However, this yielded extremely long calculation times, due to the large number of electrons to follow, with rather low energies in the bulk plasma (typical electron densities are about $10^{12}-10^{13}\,\mathrm{cm}^{-3}$).[23] Similarly, a particle-in-cell model developed previously[40] for a SiH_4/H_2 rf discharge at lower pressure (i.e., a few 100 mTorr, yielding typical electron densities of about $10^9\,\mathrm{cm}^{-3}$) could not be applied to the present conditions, due to the prohibitively long calculation times. This suggests that we need to use a hybrid Monte Carlo-fluid model. Indeed, in Ref. 35 it is stated that particle simulations and beam models are suited for modeling the directed, energetic motion of secondary electrons, but not for describing randomized, low-energy electron motion at high plasma density. A fluid model needs then to be combined to the energetic electron model to describe the latter group of electrons.[35]

Therefore, we decided to describe the α ionization due to bulk electrons in our fluid model, and to add the latter to the γ ionization calculated in our electron Monte Carlo model. Hence, this yields a two-electron-group model: the fast electrons emitted from the rf electrode are simulated with a Monte Carlo model, and the slow electrons which can, however, become slightly heated again due to the fluctuating electric field, are described with a fluid approach. The latter is justified at the rather high pressure under consideration here (about 6 Torr). In Ref. 34 a similar two-electron-group model was applied to study the transition and the occurrence of the α and γ regime. The electrons emitted from the rf electrode, as well as the ones created by ionization with sufficient kinetic+potential energy were simply considered as a monoenergetic beam. The electrons created in the plasma by ionization, or the electrons which had lost their energy by collisions in the plasma bulk, were treated as a fluid, in equilibrium with the electric field, and were described by the continuity and momentum equations. These electrons produced so-called local field ionization (i.e., the local ionization rate was only a function of the local electric field). Based on the slope of the plasma density as a function of the rf voltage, this model could make a clear distinction between the α and γ regime, in reasonable agreement with experimental observations.

In our model, a Monte Carlo model is used for the fast electrons instead of a monoenergetic beam. In the following, the hybrid model we have developed here will be described in more detail in Sec. II. Section III presents the calculation results, i.e., the electrical characteristics, potential and electric field distributions, the densities and energies of the two electron groups, and last but not least, the contributions of the various ionization mechanisms as a function of position and time in the rf cycle. Finally, the conclusions will be given in Sec. IV.

II. DESCRIPTION OF THE MODEL

A. General considerations

The species assumed to be present in the plasma are electrons, thermal argon atoms, argon ions, and fast argon atoms formed by collisions of the argon ions. These species are described by a hybrid Monte Carlo-fluid model. A Monte Carlo model is applied for the electrons emitted from the rf electrode, and for the ones created by ionization with suffi-

cient kinetic+potential energy for further ionization. When these electrons arrive in the bulk plasma and reach energies lower than the threshold for inelastic collisions (i.e., 11.55 eV for excitation to the lowest argon excited level), they are transferred to the slow electron group, which is described in a fluid model, together with the argon ions. Moreover, this fluid model also includes the Poisson equation, which allows to obtain in a self-consistent way the electric field distribution. Finally, the argon ions, which are accelerated in the sheath towards the rf electrode, are also simulated with a Monte Carlo method in this region, as well as the fast argon atoms, which are created from charge and momentum transfer collisions of the argon ions. Indeed, the argon ions and atoms can reach considerable energies in the rf sheath, and they can give rise to fast argon ion and atom impact ionization. Although the latter ionization processes are by no means dominant compared to electron impact ionization, they still play a non-negligible role in determining the electrical characteristics at the discharge conditions under study, as was demonstrated previously for an analytical dc[15] and an rf[24] discharge. These three models will be explained below in somewhat more detail.

B. Monte Carlo model for the fast electrons

The electrons start at the rf electrode during successive times in the rf cycle, as a result of the ion flux bombarding the rf electrode as a function of time in the rf cycle; the latter is calculated with the fluid model (see below). The electrons are then followed, one after the other, during successive time steps.

Their trajectory is calculated by Newton's laws

$$z = z_0 + \nu_{z_0}\Delta t + \frac{qE_{ax}(z,r,t)}{2m}(\Delta t)^2,$$

$$x = x_0 + \nu_{x_0}\Delta t + \frac{qE_{\mathrm{rad}}(z,r,t)\cos(\alpha)}{2m}(\Delta t)^2,$$

$$y = y_0 + \nu_{y_0}\Delta t + \frac{qE_{\mathrm{rad}}(z,r,t)\sin(\alpha)}{2m}(\Delta t)^2,$$

$$\nu_z = \nu_{z_0} + \frac{qE_{\mathrm{ax}}(z,r,t)}{m}\Delta t,$$

$$\nu_x = \nu_{x_0} + \frac{qE_{\mathrm{rad}}(z,r,t)\cos(\alpha)}{m}\Delta t,$$

$$\nu_y = \nu_{y_0} + \frac{qE_{\mathrm{rad}}(z,r,t)\sin(\alpha)}{m}\Delta t,$$

where z_0, x_0, y_0, and z, x, y are the position coordinates before and after Δt, v_{z_0}, v_{x_0}, v_{y_0} and v_z, v_x, v_y are the velocities before and after Δt; E_{ax} and E_{rad} are the axial and radial electric field, as a function of axial and radial position and time in the rf cycle, α is the azimuthal angle of the radial position (i.e., the angle of the radial position coordinates with respect to the x axis), and q and m are the electron charge and mass, respectively. The probability of collision during that time step is calculated by

$$\mathrm{Prob}_{\mathrm{coll}} = 1 - \exp\{-\Delta s \Sigma[n\sigma_{\mathrm{coll}}(E)]\},$$

where Δs is the distance traveled during Δt; n and $\sigma_{\mathrm{coll}}(E)$ are the densities of the target particles and the cross sections of the different collision types of the electron with energy E. A random number between 0 and 1 is generated and compared with the calculated probability of collision. If the probability is lower than the random number, no collision occurs; if the probability is higher, a collision takes place.

Collision processes incorporated in the model are total electron impact excitation from the argon atom ground state (to all excited levels), electron impact ionization of argon ground state atoms, elastic collisions with argon ground state atoms, and electron–electron Coulomb scattering. Collisions with argon ions are neglected, since these species have a much lower density than the argon atoms. The cross sections of these collisions are given in Ref. 23. In order to determine which collision takes place, the partial collision probabilities of the various collisions are calculated. The sum of these partial probabilities is, of course, equal to one. Hence, this sum is subdivided in intervals with lengths corresponding to these partial probabilities; then, a second random number between 0 and 1 is generated and the interval in which this random number falls determines the collision that takes place. The new energy and direction after the collision are then also determined by random numbers, as was explained in Ref. 23. This procedure is repeated for the next electron, and so on, until all electrons, including the ones which were formed by ionization, are simulated at this time step. Then, the next time step is simulated in the same way. When the electrons reach the bulk plasma and have energies lower than the threshold for excitation to the lowest argon excited level (i.e., 11.55 eV, which is the lowest threshold for inelastic collisions), they are transferred to the slow electron group, which is further treated in the fluid model (see below).

C. Monte Carlo model for argon ions and fast argon atoms in the rf sheath

The argon ions are generally treated sufficiently accurately with a fluid model, as is described in the next section. However, in the rf sheath the ions can reach quite high energies and produce some amount of ionization. Moreover, the atoms created from the argon ions in the rf sheath can also lead to a considerable amount of ionization. It was demonstrated before that both these processes had to be incorporated in our model, in order to be able to reproduce the correct current–voltage characteristics.[15,24] Therefore, the argon ions are also treated with a Monte Carlo model in the rf sheath, to describe explicitly the ionization processes as a function of the ion energy. Hence, it should be mentioned that these ions in the rf sheath are simulated with two models: a Monte Carlo and a fluid model. The ion densities and fluxes calculated with both models in the rf sheath are of course equal to each other. The fluid model has the advantage to insert the calculated ion density directly in Poisson's equation for a self-consistent electric field distribution. The Monte Carlo model, on the other hand, serves to calculate explicitly the ionization rate based on the ion energy.

The argon ions can enter the rf sheath from the bulk plasma (calculated from the fluid model, see below), or they can be formed in the rf sheath by γ ionization (calculated in

the above electron Monte Carlo model) or by α ionization (calculated in the fluid model, see below). All these ions are simulated in the rf sheath, as well as ions created by fast argon ion and atom impact ionization (see below). The ions are only handled with this Monte Carlo model in the rf sheath, where they can reach high energies due to the electric field and give rise to ionization; in the bulk plasma, the ions are more or less thermalized and they do not produce ionization; hence the fluid approach alone gives then all the necessary information. Moreover, the fast argon atoms formed by momentum and charge transfer collisions of the argon ions with background argon gas atoms are also treated with this Monte Carlo model.

The procedure of describing the argon ions and fast argon atoms during successive time steps is similar to the electron Monte Carlo model. They are followed, one after the other, during successive time steps. Their trajectory is calculated with Newtons' laws. Next, the probability for collision during that time step is calculated and compared to a random number, to determine whether a collision takes place or not. Collision processes taken into account in this model include symmetric charge transfer for the argon ions, and momentum transfer collisions, fast argon ion, and atom impact ionization and excitation, for both species. The kind of collision that takes place, as well as the new energy and direction after collision, are again determined by random numbers, similar to the electron Monte Carlo procedure. More information about this Monte Carlo model can also be found in Ref. 24.

D. Fluid model for the argon ions and slow electrons

At the relatively high pressure of about 6 Torr under consideration here, the slow electrons and ions can also be treated as a fluid, described with the first three moments of the Boltzmann transport equation, i.e., the balance equations for particle density, for momentum density, and for energy density.

1. Particle balance equations

The particle balance equations are as follows:

$$\frac{\partial n_{\mathrm{Ar}^+}(z,r,t)}{\partial t}+\overline{\nabla}\cdot\overline{j_{\mathrm{Ar}^+}}(z,r,t)=R_{\mathrm{Ar}^+}(z,r,t),$$

$$\frac{\partial n_e(z,r,t)}{\partial t}+\overline{\nabla}\cdot\overline{j_e}(z,r,t)=R_e(z,r,t),$$

where n_{Ar^+} and n_e are the argon ion and electron densities, $\overline{j_{\mathrm{Ar}^+}}$ and $\overline{j_e}$ are the corresponding fluxes (in vector notation), and R_{Ar^+} and R_e are the creation rates of argon ions and electrons. The creation of argon ions occurs by electron impact ionization (both calculated in the electron Monte Carlo model (γ ionization) and in the fluid model (see below; α ionization), and by fast argon ion and atom impact ionization (calculated in the ion/atom Monte Carlo model). The creation rate of the slow electrons is given by transfer to the slow electron group (obtained from the electron Monte Carlo model) and by electrons created in α ionization (calculated in the fluid model).

The ionization rate coefficient ($\mathrm{cm}^3\,\mathrm{s}^{-1}$) in the fluid model, as a function of the electron mean energy, is calculated by an empirical formula[41,42]

$$R_{\mathrm{ioniz}(\alpha)}=8.7\times10^{-9}(\epsilon-5.3)\exp\left[\frac{-4.9}{\sqrt{\epsilon-5.3}}\right],$$

where ϵ is the mean electron energy in eV. From this formula, it becomes clear that ionization can occur already for mean electron energies above 5.3 eV, although the real threshold for ionization of argon lies at 15.76 eV. Moreover, this formula predicts an increase in the ionization rate with increasing energy, whereas the cross section for electron impact ionization as a function of the electron energy reaches a maximum at around 100 eV.[43] Hence, this formula probably predicts somewhat too high ionization for higher energies than 100 eV. Since the electrons can reach energies of a few hundred eV at $\omega t=3\pi/2$ (see below; Fig. 5), the ionization calculated in the fluid model around this time might be somewhat overestimated. Nevertheless, this ionization is of minor importance compared to the high amount of ionization around $\omega t=\pi/2$ calculated in the fluid model (see below; Fig. 7), so that this approximated formula for high energies has no great effect on the overall results. By multiplying this rate coefficient with the density of electrons and argon gas atoms, the ionization rate (in $\mathrm{cm}^{-3}\,\mathrm{s}^{-1}$) can be obtained. This empirical expression agreed well with results of the kinetic model[44] and Monte Carlo[45] calculations.

2. Momentum balance equations

The momentum balance equations could be reduced to the flux equations based on diffusion and on migration in the electric field, as is explained in Ref. 42. Indeed, at the pressure under investigation here, the characteristic time between momentum transfer collisions is much smaller than the rf period, and the mean free path for these collisions is much smaller than the characteristic lengths in the discharge. This leads to the following equations:

$$\overline{j_{\mathrm{Ar}^+}}(z,r,t)=\mu_{\mathrm{Ar}^+}n_{\mathrm{Ar}^+}(z,r,t)\overline{E}^{\mathrm{eff}}(z,r,t)-D_{\mathrm{Ar}^+}\overline{\nabla}n_{\mathrm{Ar}^+}(z,r,t),$$

$$\overline{j_e}(z,r,t)=-\mu_e n_e(z,r,t)\overline{E}(z,r,t)-D_e\overline{\nabla}n_e(z,r,t),$$

where $\overline{E}$ is the electric field. Since the argon ions cannot follow the fluctuating rf electric field, they feel an effective field, $\overline{E}^{\mathrm{eff}}$, which is determined from[42]

$$\frac{\partial\overline{E}^{\mathrm{eff}}(z,r,t)}{\partial t}=\nu_m(\overline{E}-\overline{E}^{\mathrm{eff}}),$$

where ν_m is the ion momentum-transfer frequency

$$\nu_m=\frac{e}{\mu_{\mathrm{Ar}^+}m_{\mathrm{Ar}^+}}.$$

D_{Ar^+}, D_e, μ_{Ar^+} and μ_e are the argon ion and electron diffusion coefficients and mobilities, respectively. Their numerical values are taken to be the same as in Ref. 23, i.e., $D_{\mathrm{Ar}^+}=40\ \mathrm{cm}^2\,\mathrm{s}^{-1}$, $D_e=1.2\times10^6\ \mathrm{cm}^2\,\mathrm{s}^{-1}$, $\mu_c=3$

$\times 10^5\,\mathrm{cm^2\,s^{-1}\,V^{-1}}$, $\mu_{Ar^+}=1500\,\mathrm{cm^2\,s^{-1}\,V^{-1}}$ at 1 Torr and 298 K. Finally, e and m_{Ar^+} are the electronic charge and mass of the argon ion, respectively.

3. Energy balance equations

The argon ions are assumed to have thermal energies, constant in time and space, because they exchange their energy very efficiently with the background argon gas. Therefore, no energy equation is used for the argon ions. The electron energy balance equation could be written as[23]

$$\frac{\partial w_e(z,r,t)}{\partial t}+\overline{\nabla}\cdot\left(-\frac{5}{3}\mu_e w_e(z,r,t)\overline{E}(z,r,t)-\frac{5}{3}D_e\overline{\nabla}w_e(z,r,t)\right)=-e\overline{j_e}(z,r,t)\cdot\overline{E}(z,r,t)-R_{w,e}(z,r,t).$$

The term w_e is the electron energy density: $w_e=n_e\epsilon_e$, where ϵ_e is the electron energy. The second term at the left hand side describes the transport term, similar to the momentum balance equation. The first term at the right hand side describes the energy gain by the electric field (i.e., ohmic heating, $\overline{E}$ is the electric field), and the second term, $R_{w,e}$, gives the electron energy loss due to collisions (i.e., taken as the electron impact ionization rate calculated for these electrons in the fluid model, multiplied by the ionization energy).

4. Poisson's equation

Finally, the equations are coupled to Poisson's equation to obtain a self-consistent potential and electric field distribution

$$\nabla^2 V(z,r,t)+\frac{e}{\epsilon_0}(n_{Ar^+}(z,r,t)-n_e(z,r,t)-n_{e,\mathrm{MC}}(z,r,t))=0;\quad \overline{E}=-\overline{\nabla}V,$$

where ϵ_0 is the permittivity in vacuum, n_{Ar^+} and n_e are the argon ion and electron densities calculated in the fluid model, and $n_{e,\mathrm{MC}}$ is the fast electron density obtained from the Monte Carlo model.

The flux (= momentum balance) equations can be inserted into the particle continuity equations. This leads to a set of four coupled differential equations, i.e., the continuity equations for argon ions and electrons, the energy balance equation for electrons, and Poisson's equation for the electric field. Boundary conditions for these equations are taken as follows:

(1) At the rf electrode: $V(t)=V_{dc}+V_{rf}\sin(\omega_{rf}t)$, where ω_{rf} is the rf, V_{rf} is the applied rf voltage, and V_{dc} is the dc auto bias voltage developed at the rf electrode (see below).
(2) At the grounded cell walls: $V(t)=0$.
(3) $n_e=0$ at all walls and all times, because electron recombination at a conducting surface is assumed to be infinitely fast.
(4) $w_e=0$ at all walls and all times, because $w_e=n_e\epsilon_e$ (see above).
(5) $\overline{\nabla}n_{Ar^+}=0$ at all walls and all times. This means that the ion flux at the walls is only due to migration.

These four equations are strongly coupled, hence the solution was not straightforward. We used a fully implicit method, based on the Scharfetter–Gummel exponential scheme for the transport equations,[46,47] as was developed by Goedheer and co-workers.[42,48] The basic idea is that the particle fluxes are assumed constant between mesh points, instead of the densities. The advantage of this scheme is its ability to switch between situations where either the migration component or the diffusion component of the particle flux is dominant (i.e., high and low electric field, sheath region, and bulk plasma, respectively). More details about the Scharfetter–Gummel scheme can be found in Refs. 13, 42, and 48.

After discretization, the four equations are solved as a function of time. Because of the high mobility of the electrons, a fully implicit handling was found to be necessary for the electron continuity equation. Therefore, the latter equation is solved simultaneously with Poisson's equation for the self-consistent electric field at each time step, using the Newton–Raphson method. Solving both electron continuity and Poisson's equations with this method at each z and r position leads to a large bi-tridiagonal matrix (the Jacobian), which could be converted into a pentadiagonal matrix, and solved by elimination of rows. After n_e and V are known, the discretized electron energy equation is solved to obtain w_e at all z and r positions (i.e., a tridiagonal matrix). Finally, the ion continuity equation is solved (also a tridiagonal matrix) using the known values of V at that time step. When the values for all four variables at each z and r position are known at time $k+1$, the procedure is repeated for time $k+2$, etc., until steady state is reached in the periodic solution (i.e., when all variables at all z and r positions have the same value at the beginning and the end of the rf cycle).

The input parameters in the fluid model are the geometry, the boundary conditions, the pressure, and the discharge power. Moreover, initial guesses are made for the rf and dc auto bias voltages, V_{rf} and V_{dc}, which are adapted after each rf cycle. A negative dc bias voltage arises in the case of two electrodes with different size which are capacitively coupled, due to the much lower mass, and hence higher mobility, of the electrons compared to the ions. The dc bias voltage repels the electrons and attracts the ions, until steady state is reached and the total flux of electrons reaching the rf electrode during the entire rf cycle is equal to the total flux of ions. Since we are only interested in the final quasisteady state, the circuit equations are not solved in our model, but the initial dc bias is adapted after each rf cycle by the condition that the total electron flux at the rf electrode, integrated over the entire rf cycle, must be equal to the total ion flux. In practice, during each rf cycle, the total electron and ion fluxes bombarding the rf electrode are calculated. If the electron flux is lower (or higher), the value of V_{dc} is made less negative, in order to attract more electrons (or is made more negative, to repel the electrons, resp.), until both fluxes are equal to each other.

Similarly, the initial value of V_{rf} is adapted after each rf

cycle in the following way. The electrical power in the discharge can be calculated from the product of the voltage and electrical current as a function of time

$$P_{\mathrm{IV}}=\frac{1}{T}\int_0^{2\pi} V(t)\cdot I(t)dt,$$

where T is the time of the period. $V(t)$ and $I(t)$ are both calculated in the fluid model

$$V(t)=V_{\mathrm{rf}}\sin(\omega_{\mathrm{rf}}t)+V_{\mathrm{dc}},$$

$$I(t)=e[j_{\mathrm{ion,rf}}(t)-j_{\mathrm{elec,rf}}(t)]+J_D(t),$$

where $j_{\mathrm{ion,rf}}$ and $j_{\mathrm{elec,rf}}$ are the ion and electron fluxes bombarding the rf electrode (for the electrons: both the contributions of the Monte Carlo and the fluid electrons are incorporated), and J_D is the displacement current at the rf electrode (which arises from the moving of the rf sheath, and hence the change in the total positive space charge in the sheath)

$$J_D=\epsilon_0\frac{\partial E}{\partial t}.$$

By comparing this calculated P_{IV} with the input power in the model, P_{input}, the value of V_{rf} is adapted. Indeed, if $P_{\mathrm{IV}}<P_{\mathrm{input}}$, the value of V_{rf} increases by a certain amount; if $P_{\mathrm{IV}}>P_{\mathrm{input}}$, V_{rf} decreases with a certain factor, until $P_{\mathrm{IV}}=P_{\mathrm{input}}$. It should be mentioned that the value of V_{rf} can also be adapted based on the calculation of the power dissipated in the discharge by ions and electrons, as was done in Ref. 23. We tested both methods and found that they yielded the same results.

III. RESULTS AND DISCUSSION

A. Electrical characteristics

The cell geometry under consideration for this simulation is a simple cylinder with length equal to 2 cm, and diameter equal to 2.5 mm. The rf electrode is found at one side of the cylinder (hence with diameter equal to 2.5 mm), whereas the other cylinder walls are grounded. Hence, there is a large difference in size between the rf-powered and grounded electrodes. This model cell is a simplification of a real analytical rf glow discharge cell (so-called Grimm cell), for which the electrical characteristics (like power, pressure, rf amplitude, and dc bias voltages) have been measured.[49] We used the measured values of pressure (5.775 Torr) and electrical power (10.2 W) as input values, and assumed a gas temperature of 1000 K, which appears realistic for the power value under consideration.[50] Our calculated voltages will be compared with the experimental values,[49] as a means for checking the validity of our model.

Figure 1(a) presents the voltage as a function of time in the rf cycle. It is a sinusoidal profile with a negative offset of about -640 V, which is the self-consistently calculated dc bias. The rf amplitude was calculated to be 937 V. The large dc bias, which arises from the great difference in size of the rf-powered and grounded electrodes (see above), makes the voltage at the rf electrode negative during most of the rf cycle, resembling very much a dc discharge. These calculated voltage values, especially the rf amplitude, are somewhat higher than the measured values of -627 V (dc bias) and 764 V (rf amplitude), but the agreement is satisfactory. When the same discharge was operated in dc mode, at the same power, pressure, and gas temperature values, a dc voltage of 1100 V was measured. As a check, we performed similar calculations with our dc model. In this case, our model uses the voltage as an input, and the current (and hence also the electrical power) are output values. For an input value of 1100 V we obtained a current of 9.5 mA, which corresponds to an electrical power of 10.45 W, which is very close to the experimental values. Hence, from this comparison between the rf and dc mode, it follows that the rf mode requires a lower voltage for the same power, or, in other words, that the rf mode yields more efficient ionization, in agreement with experimental data. This is an important result and a validation for the present model, because the former version of our rf model (i.e., where α ionization was not correctly described) yielded the opposite result (i.e., the voltages in the rf mode were calculated to be considerably higher than in the dc mode, for the same conditions). Hence, the present correlation between calculated and experimental voltages is already satisfactory at this point; the difference can probably be attributed to model simplifications (e.g., simplified cell geometry, fluid approximation,...).

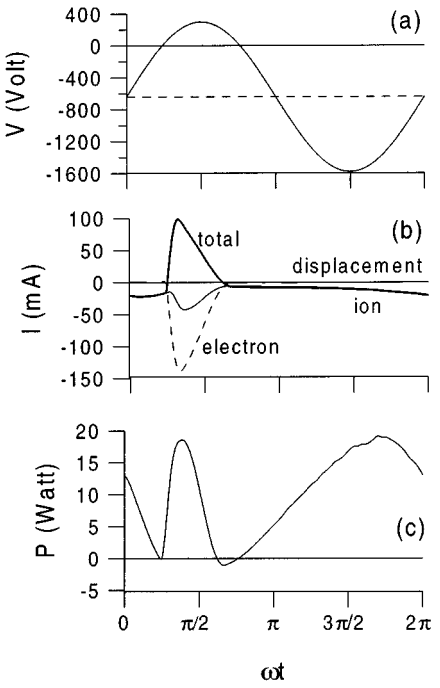

FIG. 1. Electrical potential (a), current [total current and contributions of ions, electrons, and displacement current (b)], and power (c) as a function of time in the rf cycle (at 5.775 Torr, 1000 K, 10.2 W, -640 V dc bias, and 937 V rf voltage).

The corresponding electrical current as a function of time in the rf cycle is depicted in Fig. 1(b). The individual contributions of the ion current, the electron current, and the displacement current, are also shown in Fig. 1(b). During most of the rf cycle, the ion current has the dominant contribution. Only slightly before and around $\omega t=\pi/2$, a high electron current is directed towards the rf electrode, so that at this time the total current is almost entirely determined by

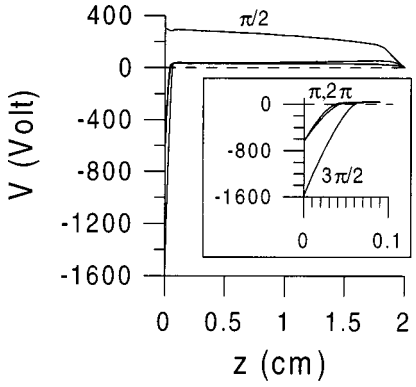

FIG. 2. One-dimensional potential distribution throughout the discharge, at four times in the rf cycle, for the same conditions as in Fig. 1. The inserted frame shows a detail of the first mm adjacent to the rf electrode.

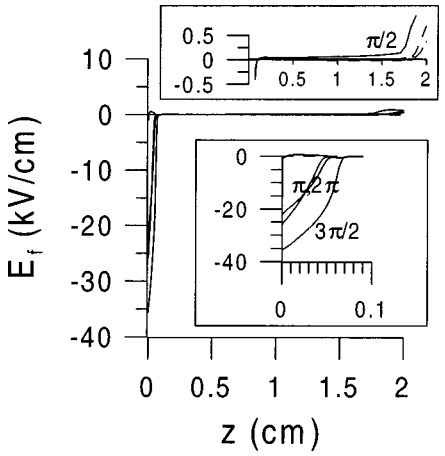

FIG. 3. One-dimensional electric field distribution throughout the discharge, at four times in the rf cycle, for the same conditions as in Fig. 1. The inserted frames show a detail of the first mm adjacent to the rf electrode and of the electric field in the bulk plasma.

this electron current. The displacement current was found to be of minor importance at the discharge conditions under study (i.e., it varies between -1 and 2 mA). This type of current is typical for rf discharges with electrodes of comparable size, where the rf sheaths change considerably in length. However, the rf discharge under study here is characterized by a large dc bias due to the great difference in size of the rf-powered and grounded electrodes (see above), so that the positive ion sheath is most of the time present in front of the rf electrode and the discharge resembles a dc discharge, where this type of current is absent. The total electrical current, integrated over the entire rf cycle, is zero, which is imposed by the capacitive coupling.

The product of both wave forms yields the power as a function of time in the rf cycle, which is illustrated in Fig. 1(c). The area under the power curve, divided by the time of the rf period, yields the calculated power of 10.2 W (see Sec. II D), as can be deduced already more or less at sight from Fig. 1(c).

The one-dimensional potential distributions along the axis of the discharge, at four times in the rf-cycle, are plotted in Fig. 2. A detail of the potential fall in the first mm adjacent to the rf electrode is included in the separate frame. At $\omega t=\pi$, $3\pi/2$, and 2π, the potential is very negative at the rf electrode, which could also be deduced from Fig. 1(a), (i.e., it is equal to the dc bias voltage at $\omega t=\pi$ and 2π, and it is equal to the sum of the dc bias and rf amplitude voltage (~ -1580 V) at $\omega t=3\pi/2$). The potential increases, however, rapidly, and goes through zero at 0.4–0.6 mm from the rf electrode, which is defined in this case as the boundary between rf sheath and bulk plasma. Further it is about 35 V in the plasma, before it returns to zero at the end of the cell, which is the grounded anode. Hence, the potential distribution at $\omega t=\pi$, $3\pi/2$, and 2π resembles very much a dc potential distribution.[13,18] At $\omega t=\pi/2$, however, the potential looks completely different. It reaches a positive value of about 300 V [i.e., the difference between rf amplitude and dc bias voltage, see Fig. 1(a)] at the rf electrode. This rather high potential is maintained through most of the rf cell, but it decreases gradually to zero at the anode walls.

From these potential distributions, the electric field distributions can also be deduced, and are shown in Fig. 3. Two frames inserted in the figure present the details of the first mm from the rf electrode and of the electric field values in the bulk plasma, respectively. It is clear that around $\omega t=\pi$, $3\pi/2$, and 2π, a very strong negative electric field is present in the rf sheath (i.e., at the rf electrode: about -20 to -25 kV/cm at $\omega t=\pi$ and 2π, and ~ -35 kV/cm at $\omega t=3\pi/2$), which accelerates the electrons away from, and the argon ions towards the rf electrode, respectively. In the bulk plasma, the electric field is very small at these times in the rf cycle. Around $\omega t=\pi/2$, however, the situation is completely different. There is only a very weak electric field in the rf sheath (strictly speaking, this region is now actually absent in front of the rf electrode), but the electric field reaches considerable values in the bulk plasma, i.e., in the order of 50–100 V/cm in the main region, increasing to almost 1 kV/cm at the grounded electrode end wall of the cylinder. This plasma bulk region can therefore, at this time in the rf cycle, be considered as an rf sheath in front of the grounded electrode. However, since the latter is much larger in size than the rf electrode, this sheath is not very localized, and the potential difference (between 300 V at the rf electrode and 0 at the grounded electrode) drops off more gradually (see Fig. 2).

B. Electron densities

Figures 4(a)–4(b) show the one-dimensional density profiles of the electrons, at four times in the rf cycle. The values are taken at the cell axis. The density of electrons treated in the fluid model (so-called slow electrons) is presented in Fig. 4(a). The densities in the rf sheath region are depicted in detail in the inserted frame. At $\omega t=\pi/2$, the density in the rf sheath is more or less constant (i.e., about $2\times 10^{11}\,\mathrm{cm}^{-3}$). This is very similar to the argon ion density in this region, so that there is more or less charge neutrality around $\omega t=\pi/2$, leading to the absence of an rf sheath. At the other times in the rf cycle, the electron density is zero in the rf sheath. Since the argon ion density is constant during the entire rf cycle, this yields a net positive space charge, giving rise to the rf sheath illustrated in Fig. 2. At the end of

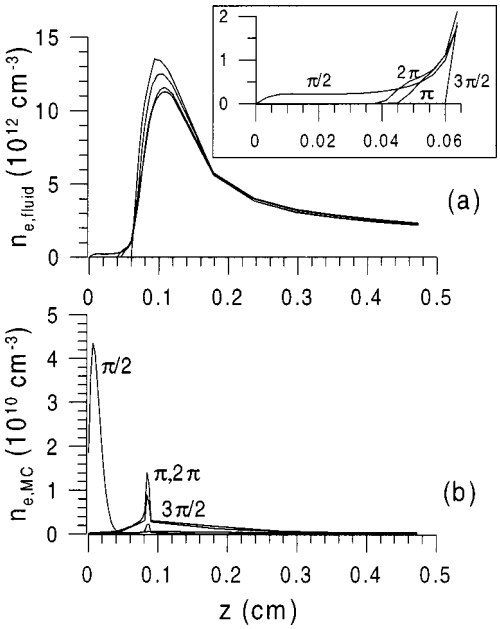

FIG. 4. One-dimensional electron density as a function of distance from the rf electrode in the first 5 mm, at four times in the rf cycle, for the same conditions as in Fig. 1, calculated with the fluid model (a) and with the Monte Carlo model (b). The inserted frame in Fig. 4(a) shows a detail of the rf sheath.

the rf sheath, the electron densities, at all times in the rf cycle, increase to high values (of $\sim 1.1-1.3\times 10^{13}\,\mathrm{cm}^{-3}$) at about 1 mm from the rf electrode. After this maximum, the electron densities decrease rather rapidly to values in the order of $10^{11}-10^{12}\,\mathrm{cm}^{-3}$ in the remaining part of the plasma. The argon ion density is very similar to the electron density in the bulk plasma, leading to nearly charge neutrality, and hence to a much lower electric field than in the rf sheath.

The electron densities calculated in our Monte Carlo model (i.e., the fast electrons), are presented in Fig. 4(b), at four times in the rf cycle (again values taken at the cell axis). The electron density values are much lower than those calculated in the fluid model, because it concerns only the fast electron group. The density is considerable, adjacent to the rf electrode at $\omega t=\pi/2$ (i.e., about $4\times 10^{10}\,\mathrm{cm}^{-3}$), because the electrons are drawn towards the rf electrode at this time, and they have rather low energies. At the other times in the rf cycle, the electron density is low at the rf electrode, but it reaches a maximum at the end of the rf sheath. If all electrons would be simulated with Monte Carlo, this electron density would further increase in the bulk plasma, and would finally even become equal to the electron density calculated in the fluid model. However, as explained in the introduction, this yielded a prohibitively long calculation time. Therefore, the electrons are transferred to the fluid model, when they reach the bulk plasma part and they have energies below 11.55 eV (see above; Sec. II B). This explains why the electron density in Fig. 4(b) drops significantly at the interface between rf sheath and bulk plasma. In fact, the sum of the electron densities of Figs. 4(a) and 4(b) yields the total electron density, which is, for example, introduced in the Poisson equation.

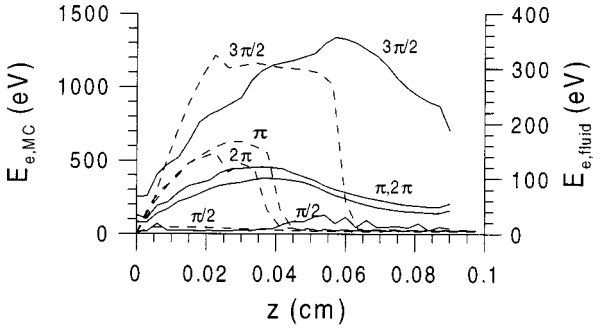

FIG. 5. One-dimensional mean electron energy as a function of distance from the rf electrode in the rf sheath, at four times in the rf cycle, for the same conditions as in Fig. 1. The energies calculated with the Monte Carlo model are presented by the solid lines (left axis), whereas the fluid results are indicated by the dashed lines (right axis).

C. Mean energies of the electrons

The mean energies of the electrons, both the ones simulated in the Monte Carlo model and the ones treated in the fluid model, are shown in Fig. 5 (again the values taken at the cell axis, and at four times in the rf cycle). The energies of the Monte Carlo electrons are presented with the solid lines, and correspond to the left *Y* axis. Only the values in the rf sheath are illustrated, because in the plasma bulk, the slow electrons disappear from this electron group, leading to an artificial increase in the mean electron energy, which can only bring confusion to the figure. At $\omega t=\pi/2$, the electron energy is less than 100 eV in the entire rf sheath. At the other times in the rf cycle, the electron energy does increase to much higher values (i.e., at $\omega t=\pi$ and 2π, the maximum is around 400 eV at 0.3–0.4 mm from the rf electrode; at $\omega t=3\pi/2$, a maximum of about 1300 eV is reached at $\sim$0.6 mm from the rf electrode), due to the energy gain from the strong electric field in front of the rf electrode. At the end of the rf sheath, the electric field is not so strong anymore, and the electrons lose their energy due to collisions, so that their mean energy decreases. This trend would continue in the bulk plasma. However, since the slow electrons are now transferred to the fluid model, the mean (fast) electron energy apparently increases again.

The mean energies of the electrons treated in the fluid model, at four different times in the rf cycle, are represented by the dashed lines and the right *Y* axis in Fig. 5. Again, only the values in the rf sheath are shown; the values in the bulk plasma are more or less constant (see below). At $\omega t=\pi/2$, the mean energy is again rather low in the rf sheath, because the electrons are not accelerated by a very strong electric field in the rf sheath. It increases from about 5 eV at the boundary between the rf sheath and plasma bulk to $\sim$10 eV at the rf electrode. In the bulk plasma, the electron energy increases again slightly, due to the moderate electric field in this region and at this time (see Fig. 3). However, because the energy gain by the moderate electric field is more or less balanced by the energy loss due to collisions, the electron energy remains about 7–8 eV. At the end of the discharge region, the electric field is somewhat higher (see Fig. 3), and the electron energy increases to values of about 17 eV. At the other times in the rf cycle, the electron energy reaches again

rather high values in the rf sheath, i.e., about 140–170 eV at $\omega t = \pi$ and 2π; and ~300 eV at $\omega t = 3\pi/2$. It should, however, be mentioned that these rather high mean energies correspond only to a limited number of electrons (see the low electron densities in the rf sheath, calculated in the fluid model, as was shown in Fig. 4).

From Fig. 5 it becomes clear that the maximum energy of the fluid electrons is somewhat lower than for the Monte Carlo electrons. Indeed, the Monte Carlo electrons were emitted from the rf electrode and traverse the entire rf sheath, so that, if they would undergo no collisions, they could gain energy equal to the total potential drop. The fluid electrons, on the other hand, were originally slow electrons in the bulk plasma, which have been drawn towards the rf electrode around $\omega t = \pi/2$. A fraction of these electrons can really reach the rf electrode; the remaining fraction will be overtaken by the moving rf sheath at times later than $\omega t = \pi/2$, before they can reach the rf electrode, and they will be reaccelerated away from the rf electrode by the strong electric field which again dominates now in the rf sheath. Therefore, unlike the electrons emitted from the rf electrode, these electrons do not necessarily traverse the entire rf sheath, and they can gain kinetic energy corresponding to only a fraction of the total potential drop. Hence, the mean energy of these electrons is lower than the electrons emitted from the rf electrode, which are simulated in the Monte Carlo model. In the bulk plasma, the electrons lose their energy further by collisions, and they cannot gain much energy from the weak electric field. Therefore, their mean energy decreases to values of a few eV in the bulk plasma. Because the electrons in the fluid model can only give rise to ionization if their mean energy is above 5.3 eV (see Sec. II C), it is expected that the fluid electrons will contribute to ionization in the rf sheath, but not in the bulk plasma, except around $\omega t = \pi/2$, where the electric field is sufficiently high to supply the required energy to the electrons for ionization. This will be discussed in the next section.

D. Contributions of the ionization processes

Figures 6(a)–6(b) present the one-dimensional ionization rates calculated at four times in the rf cycle, with our Monte Carlo model [Fig. 6(a)] and our fluid model [Fig. 6(b)]. The ionization rate computed in the Monte Carlo model corresponds actually to γ ionization, because it is produced by electrons emitted from the rf electrode due to argon ion bombardment, and by electrons created in collisions from these first electrons, before they are slowed down in the bulk plasma. Around $\omega t = \pi$, $3\pi/2$, and 2π the ionization rate reaches a maximum at the boundary between rf sheath and bulk plasma, where the electrons reach high energies. The γ ionization seems to be less efficient around $\omega t = 3\pi/2$, because the maximum mean electron energy (about 1300 eV; see Fig. 5) is clearly above the energy corresponding to maximum in the cross section curve (i.e., ~100 eV).[43] At $\omega t = \pi/2$, the ionization rate reaches its maximum very close to the rf electrode, because the electrons are generally directed towards the rf electrode around this time in the rf cycle. Further than about 0.5 mm from the rf electrode, the γ ionization at $\omega t = \pi/2$ appears to be negligible, so that the overall ionization around $\omega t = \pi/2$ is much lower than at the other times in the rf cycle.

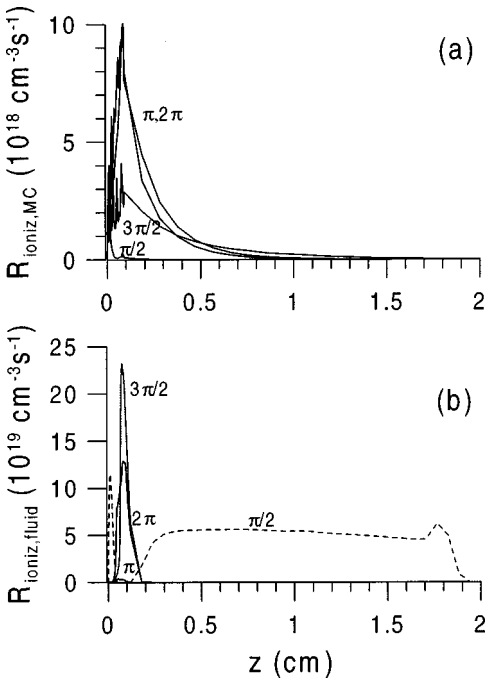

FIG. 6. One-dimensional electron impact ionization rates throughout the discharge, at four times in the rf cycle, for the same conditions as in Fig. 1, calculated in the Monte Carlo model [γ ionization; figure (a)] and in the fluid model [α ionization; figure (b)].

This is, however, not true for the ionization calculated in our fluid model, which corresponds to α ionization, i.e., ionization produced by slow electrons which can again become heated by the fluctuating electric field. It should be mentioned that the ionization calculated in the fluid model consists, actually, of two mechanisms: (i) the ionization produced by slow plasma bulk electrons which become again heated by the sheath expansion (so-called ''wave-riding'' electrons), and (ii) the ionization produced by slow bulk electrons which can be slightly heated by the moderate electric field in the plasma bulk around $\omega t = \pi/2$. Strictly speaking, only the first mechanism is generally called α ionization. The second mechanism is sometimes compared to positive column ionization,[30] where a moderate electric field is also present to compensate for electron losses to the walls. In our case, the latter mechanism is especially important around $\omega t = \pi/2$; the moderate electric field, however, does not arise as a compensation for electron losses to the walls, but it results from the potential drop of 300 V at the rf electrode to zero at the grounded electrode. It can therefore be considered as ionization in the (large but diffuse) sheath, which is present in front of the grounded electrode at $\omega t = \pi/2$.

As follows from Fig. 6(b), the ionization around $\omega t = \pi/2$ (dashed line) shows indeed two peaks, a sharp one adjacent to the rf electrode (since the electrons move towards the rf eletrode at this time of the rf cycle), and a very broad one in the bulk plasma. Indeed, as was mentioned above, the mean electron energy in this region was calculated to be about 7–8 eV, which is found to be sufficient to yield ion-

ization throughout the entire bulk plasma. At the end of the discharge region, there is even a small maximum, which corresponds to the higher electron energy, resulting from the somewhat higher electric field. Since this high value of ionization is maintained throughout the entire bulk plasma, the overall ionization at this time in the rf cycle is considerably large, as will also become clear from Fig. 7 (see below). At the other times in the rf cycle [see Fig. 6(b), solid lines], the ionization reaches again its maximum at the boundary between the rf sheath and bulk plasma, where the electrons have their maximum energy. Now, the ionization appears to be most efficient around $\omega t = 3\pi/2$, since the fluid electrons have in general lower energies than the Monte Carlo electrons (see Fig. 5), and the energies around $\omega t = 3\pi/2$ can yield the most efficient ionization, according to the empirical formula given in Sec. II C. At $\omega t = \pi$, the ionization is clearly lower. This follows from the combination of Figs. 4(a) and 5. Indeed, the electron density is very low until 0.45 cm from the rf electrode [Fig. 4(a)] and the electron mean energy has already decreased to low values at this position (Fig. 5). Due to the approximation of the threshold mean energy of 5.3 eV in the empirical formula for ionization in the fluid model, electrons with lower mean energy can yield no ionization. It is possible that the ionization calculated with the fluid model around $\omega t = \pi$ should be higher than indicated in Fig. 6(a) (i.e., more comparable to the ionization around $\omega t = 2\pi$), if another approximation is applied for the empirical formula in the fluid model. However, as will be shown in Fig. 7 (see below), the ionization both around $\omega t = \pi$ and $\omega t = 2\pi$ is of minor importance compared to the ionization around $\omega t = \pi/2$, and hence, it will not influence the calculated electrical parameters.

Beside the electrons, the fast argon ions and atoms can also contribute to ionization in the rf-sheath where they can reach rather high energies (see also Refs. 15 and 24). The ionization due to both argon species reaches a maximum at the rf electrode, where the ions and atoms reach maximum energies. The rates of these ionization processes are in the order of 10^{18}–$10^{19}\,\mathrm{cm}^{-3}\,\mathrm{s}^{-1}$, which is comparable to electron impact ionization, both calculated in the electron Monte Carlo model and in the fluid approach [see Figs. 6(a) and 6(b)]. However, ion and atom impact ionization occur only in a small region very close to the rf electrode, so that the overall contribution of these processes to the total ionization in the discharge will be of minor importance (see below).

The individual contributions of argon ionization, attributed to the different sources (i.e., γ electron impact ionization calculated in the electron Monte Carlo model, α electron impact ionization treated in the fluid model, and fast argon ion and atom impact ionization simulated in the fast argon ion and atom Monte Carlo model), integrated over the entire discharge region, are plotted as a function of time in the rf cycle in Fig. 7. Moreover, the total amount of ionization is also illustrated. From this figure it becomes clear that α ionization (i.e., calculated in the fluid model; long dashed line) has the largest contribution in the overall ionization, mainly due to the large amount around $\omega t = \pi/2$. The total contribution, integrated over the entire rf cycle, amounts to almost 72%. The γ ionization (computed in the electron Monte Carlo model; short dashed line) contributes to about 23%, when integrated over the entire rf cycle; it is at its maximum around $\omega t = 2\pi$ and at its minimum around $\omega t = \pi/2$. Fast argon ion and atom impact ionization, which are presented as a function of time in the lower part of Fig. 7, have only a minor contribution (i.e., integrated over the entire discharge region and rf cycle, about 1% and 4%, respectively). However, as was demonstrated in Ref. 24, their contribution plays a non-negligible role in determining the electrical characteristics at the rather high voltages under consideration here, because their ionization creates more electrons, which produce in turn also more ionization, etc. (like a snowball effect).

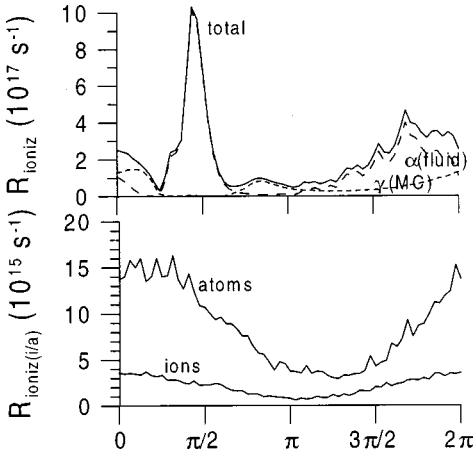

FIG. 7. Total ionization rate and contributions of the different mechanisms, integrated over the entire discharge region, as a function of time in the rf cycle, for the same conditions as in Fig. 1. The upper part of the figure presents the total electron ionization (solid line) and the contributions by α (long dashed line) and γ (short dashed line) ionization (calculated in the fluid and Monte Carlo model, resp.). The lower part shows the ionization rate by fast argon ion and atom impact ionization.

IV. CONCLUSION

We have developed a hybrid Monte Carlo-fluid model for the description of electrons, argon ions, and fast argon atoms in a capacitively coupled rf glow discharge used in analytical spectroscopy. Since the latter operates at rather high pressures (e.g., about 6 Torr) and high powers (e.g., ~10 W for a small cell with a diameter of only 2.5 mm), the electron densities can become quite large (i.e., $10^{13}\,\mathrm{cm}^{-3}$). The computation time to simulate all these electrons with a Monte Carlo or a particle-in-cell method was found to be prohibitively long. Therefore, only the fast electrons, emitted from the rf electrode, and the ones produced by ionization collisions with sufficiently high energies, were treated with the Monte Carlo method (roughly called γ ionization). The slow electrons in the bulk plasma, which can, however, be heated again by the fluctuating rf electric field and which can then again cause some ionization (so-called α ionization), are described with a fluid approach. The latter method is justified for these slow electrons at the rather high pressures under consideration here, and it is considerably faster than a pure

Monte Carlo or a particle-in-cell method. However, special attention must be paid to the exact bookkeeping of the electrons, i.e., it must be ensured that all electrons are correctly treated, with only one model, and that they do not contribute twice to the ionization. Moreover, another Monte Carlo model is applied to simulate the behavior of fast argon ions and atoms in the rf sheath, because they play a non-negligible role in determining the electrical characteristics.

When the gas pressure and temperature and the electrical input power are given, the rf amplitude and dc bias voltages could be calculated, and they agree reasonably well with measured values. Moreover, we found that the ionization in the rf discharge was more efficient than in the dc discharge, or in other words, that the rf discharge required lower voltages than the dc discharge, for the same power, which is also in good correspondence to the experimental data. It should be mentioned that this was not the case with a previous version of our hybrid Monte Carlo-fluid model, where the electron impact ionization was only calculated with the Monte Carlo method.

Other results of this model, which have been presented in this article, include the potential and electric field distributions, the electron densities, and the mean electron energies, both of the Monte Carlo electrons and the fluid electrons.

Finally, last but not least, the contributions of the various ionization mechanisms (i.e., electron impact γ and α ionization, and fast argon ion and atom impact ionization) have been determined. The latter two ionization processes are nearly negligible at the conditions under study, although it was demonstrated in Refs. 15 and 24 that they still play a role in determining the electrical characteristics. However, both α and γ electron impact ionization play an important role in the investigated discharge conditions, with an overall contribution of about 72% and 23%, respectively. The dominant role of α ionization is mainly attributed to its contribution around $\omega t = \pi/2$. Indeed, although the electrons have rather low energies in the bulk plasma, the electric field in this region around $\omega t = \pi/2$ is still sufficiently high to heat these electrons to energies just high enough to produce ionization. The fact that the latter ionization mechanism was not correctly described in a previous version of our hybrid Monte Carlo-fluid model[23] explains why we could not predict the experimentally observed difference in electrical characteristics between glow discharges in the dc mode and in the rf mode. With the present model, we are able to predict this experimental difference. A more detailed comparison between a glow discharge in the dc and the rf mode will be carried out in the near future.[51]

ACKNOWLEDGMENTS

A. Bogaerts is indebted to the Flemish Fund for Scientific Research (FWO) for financial support. M. Yan is financed by a New Research Initiative of the University of Antwerp. The research of W. Goedheer is financed by the ''Stichting voor Fundamenteel Onderzoek der Materie.'' The authors also acknowledge financial support from the Federal Services for Scientific, Technical and Cultural Affairs (DWTC/SSTC) of the Prime Minister's Office through IUAP-IV (Conv. P4/10). Finally, A. Bogaerts wishes to thank V. Hoffmann for supplying the experimental data and other helpful information, and Ph. Belenguer for the interesting discussions about α and γ ionization.

[1] D. C. Duckworth and R. K. Marcus, Anal. Chem. **61**, 1879 (1989).
[2] C. Lazik and R. K. Marcus, Spectrochim. Acta B **48**, 1673 (1993).
[3] R. K. Marcus, T. R. Harville, Y. Mei, and C. R. Shick, Jr., Anal. Chem. **66**, 902A (1994).
[4] F. Prässler, V. Hoffmann, J. Schumann, and K. Wetzig, J. Anal. At. Spectrom. **10**, 677 (1995).
[5] S. De Gendt, R. Van Grieken, W. Hang, and W. W. Harrison, J. Anal. At. Spectrom. **10**, 689 (1995).
[6] A. I. Saprykin, J. S. Becker, and H.-J. Dietze, J. Anal. At. Spectrom. **10**, 897 (1995).
[7] M. J. Heintz and G. M. Hieftje, Spectrochim. Acta B **50**, 1125 (1995).
[8] V. Hoffmann, H.-J. Uhlemann, F. Prässler, K. Wetzig, and D. Birus, Fresenius J. Anal. Chem. **355**, 826 (1996).
[9] R. K. Marcus, J. Anal. At. Spectrom. **11**, 821 (1996).
[10] X. Pan, B. Hu, Y. Ye, and R. K. Marcus, J. Anal. At. Spectrom. **13**, 1159 (1998).
[11] A. Perez, R. Pereiro, N. Bordel, and A. Sanz-Medel, Spectrochim. Acta B **53**, 1541 (1998).
[12] A. Bogaerts, M. van Straaten, and R. Gijbels, Spectrochim. Acta B **50**, 179 (1995).
[13] A. Bogaerts, R. Gijbels, and W. J. Goedheer, J. Appl. Phys. **78**, 2233 (1995).
[14] A. Bogaerts and R. Gijbels, Phys. Rev. A **52**, 3743 (1995).
[15] A. Bogaerts and R. Gijbels, J. Appl. Phys. **78**, 6427 (1995).
[16] A. Bogaerts, M. van Straaten, and R. Gijbels, J. Appl. Phys. **77**, 1868 (1995).
[17] A. Bogaerts and R. Gijbels, J. Appl. Phys. **79**, 1279 (1996).
[18] A. Bogaerts, R. Gijbels, and W. J. Goedheer, Anal. Chem. **68**, 2296 (1996).
[19] A. Bogaerts and R. Gijbels, Anal. Chem. **68**, 2676 (1996).
[20] A. Bogaerts and R. Gijbels, J. Anal. At. Spectrom. **12**, 751 (1997).
[21] A. Bogaerts, R. Gijbels, and J. Vlcek, J. Appl. Phys. **84**, 121 (1998).
[22] A. Bogaerts, R. Gijbels, and R. J. Carman, Spectrochim. Acta B **53**, 1517 (1998).
[23] A. Bogaerts, R. Gijbels, and W. J. Goedheer, Jpn J. Appl. Phys. (in press).
[24] A. Bogaerts and R. Gijbels, IEEE Trans. Plasma Sci. (in press).
[25] B. Chapman, *Glow Discharge Processes* (Wiley, New York, 1980).
[26] W. W. Harrison and B. L. Bentz, Prog. Anal. Spectrosc. **11**, 58 (1988).
[27] S. M. Levitskii, Sov. Phys. Tech. Phys. **2**, 887 (1958).
[28] N. A. Yatsenko, Sov. Phys. Tech. Phys. **25**, 1454 (1980).
[29] V. A. Godyak and A. S. Kanneh, IEEE Trans. Plasma Sci. **PS-14**, 112 (1986).
[30] M. J. Kushner, IEEE Trans. Plasma Sci. **PS-14**, 188 (1986).
[31] Y. P. Raizer and M. N. Schneider, Sov. J. Plasma Phys. **13**, 267 (1987).
[32] P. Vidaud, S. M. A. Durrani, and D. R. Hall, J. Phys. D **21**, 57 (1988).
[33] J. Perrin, P. Roca, I. Cabarrocas, B. Allain, and J. M. Freidt, Jpn. J. Appl. Phys., Part 1 **27**, 2041 (1988).
[34] Ph. Belenguer and J. P. Boeuf, Phys. Rev. A **41**, 4447 (1990).
[35] T. J. Sommerer, W. N. G. Hitchon, R. E. P. Harvey, and J. E. Lawler, Phys. Rev. A **43**, 4452 (1991).
[36] M. Surendra and D. B. Graves, IEEE Trans. Plasma Sci. **PS-19**, 144 (1991).
[37] V. A. Godyak, R. B. Piejak, and B. M. Alexandrovich, Phys. Rev. Lett. **68**, 40 (1992).
[38] C. Li and C.-H. Wu, IEEE Trans. Plasma Sci. **PS-20**, 1000 (1992).
[39] S. V. Berezhnoi, I. D. Kaganovich, M. Misina, A. Bogaerts, and R. Gijbels, IEEE Trans. Plasma Sci. (in press).
[40] M. Yan and W. J. Goedheer, Plasma Sources Sci. Technol. **8**, 349 (1999).
[41] A. D. Richards, B. E. Thompson, and H. H. Sawin, Appl. Phys. Lett. **50**, 492 (1987).
[42] J. D. P. Passchier, Ph.D. thesis, University of Utrecht, 1994.
[43] R. J. Carman, J. Phys. D **22**, 55 (1989).
[44] P. M. Meijer, W. J. Goedheer, and J. D. P. Passchier, Phys. Rev. A **45**, 1098 (1992).
[45] M. S. Barnes, T. J. Cotler, and M. E. Elta, J. Comput. Phys. **77**, 53 (1988).
[46] H. K. Gummel, IEEE Trans. Electron Devices **11**, 455 (1964).

[47] D. L. Scharfetter and H. K. Gummel, IEEE Trans. Electron Devices **16**, 64 (1969).
[48] J. D. P. Passchier and W. J. Goedheer, J. Appl. Phys. **74**, 3744 (1993).
[49] V. Hoffmann (unpublished results).
[50] N. P. Ferreira, H. G. C. Human, and L. R. P. Butler, Spectrochim. Acta B **35B**, 287 (1980).
[51] A. Bogaerts, R. Gijbels, and W. J. Goedheer, Spectrochim. Acta B (in press).